International Journal of Pharmaceutics 664 (2024) 124623

Contents lists available at ScienceDirect

International Journal of Pharmaceutics

journal homepage: www.elsevier.com/locate/ijpharm

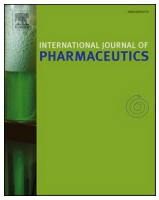

Prostate cancer chemotherapy by intratumoral administration of Docetaxel-Mesoporous silica nanomedicines

Eva Rivero-Buceta [a,1], Adrián Bernal-Gómez [b,c,1], Carla Vidaurre-Agut [a], Eric Lopez Moncholi [d], Jose María Benlloch [e], Victoria Moreno Manzano [d], César David Vera Donoso [b,c], Pablo Botella [a,*]

[a] Instituto de Tecnología Química (UPV–CSIC), Universitat Politècnica de València–Consejo Superior de Investigaciones Científicas, Avda. de los Naranjos s/n, 46022 València, Spain
[b] Escuela de Doctorado, Universidad Católica de Valencia, Plaza de San Agustín 3, 46001 Valencia, Spain
[c] Hospital Universitario y Politécnico La Fe, Av. Fernando Abril Martorell, 106, 46026 Valencia, Spain
[d] Centro Investigación Príncipe Felipe, C/Eduardo Primo Yúfera 3, Valencia 46012, Spain
[e] Instituto de Instrumentación para Imagen Molecular (I3M), Centro Mixto CSIC-Universitat Politècnica de Valencia, Camino de Vera s/n, 46022 Valencia, Spain

ARTICLE INFO

Keywords:
Prostate cancer
Intratumoral administration
Mesoporous silica nanoparticles
Docetaxel

ABSTRACT

Docetaxel (DTX) is a recommended treatment in patients with metastasic prostate cancer (PCa), despite its therapeutic efficacy is limited by strong systemic toxicity. However, in localized PCa, intratumoral (IT) administration of DTX could be an alternative to consider that may help to overcome the disadvantages of conventional intravenous (IV) therapy. In this context, we here present the first *in vivo* preclinical study of PCa therapy with nanomedicines of mesoporous silica nanoparticles (MSN) and DTX by IT injection over a xenograft mouse model bearing human prostate adenocarcinoma tumors. The efficacy and tolerability, the biodistribution and the histopathology after therapy have been investigated for the DTX nanomedicine and the free drug, and compared with the IV administration of DTX. The obtained results demonstrate that IT injection of DTX and DTX nanomedicines allows precise and selective therapy of non-metastatic PCa and minimize systemic diffusion of the drug, showing superior activity than IV route. This allows reducing the therapeutic dose by one order and widens substantially the therapeutic window for this drug. Furthermore, the use of DTX nanomedicines as IT injection promotes strong antitumor efficacy and drug accumulation at the tumor site, improving the results obtained with the free drug by the same route.

1. Introduction

Prostate cancer (PCa) is the second most commonly diagnosed cancer in men, with an estimated 1.5 million (7.3 % of cases) diagnoses worldwide in 2022 (WHO). Prevalence of PCa by age > 79 years is 59 % among men > 79 years. Despite the advances in recent decades, PCa chemotherapy presents important limitations yet (Ferlay et al., 2015). Here, docetaxel (DTX) is a semisynthetic anticancer agent of the taxoid family, which is well-known for its antitumor activity against various types of cancers (e.g., gastric, breast, lung, ovarian) (Crown et al., 2004; Engels et al., 2007; He et al., 2015; Kaye et al., 1995) and recommended as optional treatment in patients with metastasic prostate cancer (Engels et al., 2005; Petrylak, 2006). However, the therapeutic efficacy of DTX is hampered by its systemic toxicity, which conditions the dose and number of chemotherapy cycles, as well as the development of resistance by tumor cells (Geney et al., 2002). Furthermore, molecular features of DTX such as size, circulation in blood bound to proteins and low solubility make difficult to achieve an adequate biodistribution.

At this point, local treatment of PCa has emerged as an alternative to overcome the disadvantages of conventional intravenous (IV) therapy, although the consolidation of these protocols still needs of additional clinical evidence (Tilki et al., 2018; Yoo et al., 2010). In this sense, the intratumoral (IT) administration of cytotoxic drugs has been widely studied with the aim of imposing stronger antitumor action with lower systemic diffusion and fewer adverse effects, as well as avoiding the development of drug resistances (Walter et al., 1995; Goldberg et al., 2010;) (Jiang et al., 2024; Shaha et al., 2024). Furthermore, this IT route was presumed to be particularly advantageous in chemotherapy-

* Corresponding author.
E-mail address: pbotella@itq.upv.es (P. Botella).
[1] These authors contributed equally to this work and should be regarded as co-first authors.

https://doi.org/10.1016/j.ijpharm.2024.124623
Received 31 May 2024; Received in revised form 18 August 2024; Accepted 19 August 2024
Available online 25 August 2024

resistant cancers such as central nervous system tumors. In addition, infusion of chemotherapy to treat brain tumors can be considered a form of intra-tumoral injection (D'Amico et al. 2020; Virtanen et al. 2024). Although promising from a conceptual point of view, almost no IT chemotherapy protocol has been successfully translated into real daily practice, apart from the endoscopic administration of IT chemotherapy in some scenarios of lung cancer (Celikoglu et al., 2008; Mohan et al., 2018).

For instance, the IT administration of DTX in a xenograft mouse model of head and neck cancer, allowed to achieve maximum concentrations of the drug in tumor three orders higher than conventional IV dosing (Yoo et al., 2005). In addition, the IT administration of DTX nanoparticles has shown an important benefit in retaining the drug within the tumor, both in preclinical and clinical investigations, allowing longer residence times and acting as a drug depot, which exposes the chemotherapeutic molecule to tumor cells for several weeks without contributing to systemic toxicity (Maulhardt et al., 2023, 2021, 2019).

In this context, we recently have shown that mesoporous silica nanoparticles (MSNs) are promising nanocarriers for DTX delivery to prostate cancer cells, due to their biocompatibility, large surface area, tailorable pore size and easy functionalization with organic moieties (Rivero-Buceta et al., 2019). Specific engineered chemical modifications of MSNs (e.g., incorporation of amino groups) result in functional and biocompatible nanocarriers. In addition, MSNs have recently shown significant advances in the fields of biotechnology (Mazzotta et al., 2022), peptide-driven nanoparticles (Cavallaro et al., 2023), nanodynamic therapies (Xu et al., 2022), immunological studies (Escriche-Navarro et al., 2022) and perspectives in multitargeting molecular therapies (Puzzo et al., 2024). The recent approval by the Food and Drug Administration (FDA) of "silica nanoparticles" for specific clinical applications has boosted the potential of this vehicle for the development of novel drug delivery systems (DDSs) (Bobo et al., 2016). The irruption of nanomedicines can provoke also significant evolution for IT chemotherapy. Thanks to their versatility and chemical characteristics, conjugation to nanomedicines could improve retention of cytotoxic molecules in the tumor site after IT administration and enhance their intracellular intake, among other effects (Yun et al., 2023).

In this work we present the first *in vivo* preclinical study of PCa therapy with nanomedicines of MSN and DTX by IT administration over a xenograft mouse model. The efficacy and tolerability, the biodistribution and the histopathology after IT administration in athymic nude male mice bearing human prostate adenocarcinoma tumors have been investigated for the nanomedicine and the free DTX, and compared with the IV injection of DTX. The results show the potential of combining DTX nanomedicines with IT route for efficient antitumor therapy.

2. Materials and methods

2.1. Reagents, cells and animals

DTX was purchased from Carbosynth. All chemical reagents were obtained from Sigma-Aldrich (St. Louis, MO, USA), except HATU (Fluorochem, Hadfield, UK). UPLC grade solvents were supplied by Scharlab (Barcelona, Spain). Water was deionized to 18.2 MΩ cm^{-1} by using a milliQ pack system.

Human prostate cancer cell line LNCaP was originally obtained from ATCC (Rockville, MD, USA), and maintained at 37 °C under a humified atmosphere of 95 % air and 5 % CO_2 in RPMI 1640 medium (Lonza, Verviers, Belgium) supplemented with 10 % FBS (Sigma-Aldrich). A combination of Penicillin/Streptomycin acquired from GE Healthcare HyClone was used to preclude microbial growth. Trypsin-EDTA 0.25 % was obtained from Merck Millipore and used to remove adherent cells from a culture surface.

A human s.c. prostate cancer mouse model was developed from male athymic nude mice (4 weeks old, CR athymic HO mouse nu/nu, Charles River Laboratories, Saint Germain Nuelles, France). Mice were kept in pathogen-free conditions and used at 6 weeks of age. Animals were housed in separate cages (4 animals per cage), maintained in a controlled atmosphere with 12-hour light/dark cycles and free access to food and water. Animal care and experimental procedures were carried out in accordance to guidelines for the Ethics Committee (CEEA) of the Hospital Universitario y Politécnico La Fe. After 10–14 days for settling, 3×10^6 LNCaP cells suspended into 100 μL sterile mixture (50 μL complete culture medium and 50 μL Matrigel™) was injected s.c. into the right flank of the mice. Tumor growth was monitored every four days for 6–8 weeks by conventional caliper measurements. When the tumor volume averaged 255 mm^3, mice were randomized into six groups (5 mice per group). Tumor volume was calculated by using the Eq. (1):

$$Tumor\ volume\ (mm^3) = \frac{Dxd^2}{2} \quad (1)$$

where D and d (in mm) are, respectively, the major and minor diameter of the tumor.

2.2. Synthesis and characterization of docetaxel nanomedicine

DTX nanomedicine (MNX) is based on mesoporous silica nanoparticles loaded with 2′-hemisuccinate docetaxel. All synthetic protocols were carried out according to a previous protocol of our group (see Supplementary Information) (Cai et al., 2001; Liu et al., 2013; Rivero-Buceta et al., 2019).

The as-synthesized nanoparticle morphology was examined by transmission electron microscopy (TEM) in a JEOL JEM 2100F microscope operating at 200 kV. The size distribution of as-synthetized nanoparticles in aqueous dispersions was determined using a Zetasizer Nano ZS (Malvern Instruments Ltd., Worcestershire, United Kingdom). Here, suspensions of dried materials at a concentration of 5 μg/mL were prepared and dynamic light scattering (DLS) measurements were performed at pH 7, 25 °C and 173° scattering angle. Moreover, Zeta determinations were conducted at pH 7 and 25 °C with the same equipment. The dried material was resuspended in deionized water at a concentration of 5 μg/mL. The mean hydrodynamic diameter was determined by cumulant analysis. Powder X-ray diffraction (XRD) patterns were collected in a Philips X'Pert diffractometer equipped with a graphite monochromator, operating at 40 kV and 45 mA. Nitrogen gas adsorption isotherms were measured in a Micromeritics Flowsorb apparatus. Surface area calculations were performed using the BET method (Barrett et al., 1951), and pore size distribution was determined according to the KJS estimation (Kruk et al., 1997). Carbon content in nanoparticles corresponding to the organic functionalization was monitored by elemental analysis (FISONS, EA 1108 CHNS-O). The drug loading efficiency in the nanoparticles was calculated according to Eq. (2):

$$DTX\ Loading\ Efficiency\ (\%) = \frac{Total\ amount\ of\ drug\ conjugated\ in\ nanoparticles}{Total\ amount\ of\ drug\ added\ initially} x100 \quad (2)$$

2.3. In vivo testing: Tolerability and efficacy

LNCaP tumor-bearing mice were randomized based on tumor volume to six groups (n = 5/group). The treatments were administered *via* IT or IV injection. In case of IT administration, we first studied the optimum dosage by injecting the free drug at a low dose (2 mg DTX kg^{-1}; D1 group) and a high dose (10 mg DTX kg^{-1}; D2 group). A control IT group (C1 group) received only the vehicle. Subsequently, we decided to administer DTX nanomedicine at the lowest DTX equivalent concentration (2 mg DTX equivalent kg^{-1}; N1 group). Conversely, the groups of IV administration were: D3 (2 mg DTX kg^{-1}) and C2 (control, vehicle). The vehicle in all cases was an isotonic glucose solution (ethanol:tween 80:glucose 5 % 1:1:8 v/v/v, see Supplementary Information). IV administration was carried out through the tail vein. In all cases the injected volume was 100 μL. However, when the tumor volume dropped below 100 mm^3, the injected volume was limited to 50 μL, also recalculating drug concentration in order to keep the assigned dose. All groups were treated at the same dosing schedule: every 4 days, up to 16 days.

Tumor size and body weight were recorded along the experiment according to dosing schedule. The tumor volume and the body weight treatment to control (T/C) values were calculated by dividing median values at the end of the treatment with those at initiation of the treatment and referring treatment groups to ratios in control (vehicle) groups (see Eqs. (3) and (4)).

$$\frac{T}{C}\ Body\ Weight\ equation = \left(\frac{\frac{median\ of\ animal\ weight\ at\ the\ end\ of\ the\ treatment\ with\ DTX\ or\ MNX}{median\ of\ animal\ weight\ before\ the\ treatment\ with\ DTX\ or\ MNX}}{\frac{median\ of\ animal\ weight\ at\ the\ end\ of\ the\ treatment\ with\ vehicle}{median\ of\ animal\ weight\ before\ the\ treatment\ with\ vehicle}} \times 100 \right) - 100 \quad (3)$$

$$\frac{T}{C}\ Tumor\ Volume\ equation = \left(\frac{\frac{median\ of\ tumor\ volume\ at\ the\ end\ of\ the\ treatment\ with\ DTX\ or\ MNX}{median\ of\ tumor\ volume\ before\ the\ treatment\ with\ DTX\ or\ MNX}}{\frac{median\ of\ tumor\ volume\ at\ the\ end\ of\ the\ treatment\ with\ vehicle}{median\ of\ tumor\ volume\ before\ the\ treatment\ with\ vehicle}} \right) \quad (4)$$

At the end of the experiment (24 h after last injection) mice were euthanized by CO_2 overdose, and blood was collected from the inferior vena cava and stored in an Eppendorf tube with heparin sodium. This sample was centrifuged at 9,300 rcf for 10 min. Subsequently, the plasma was collected and immediately stored at −80 °C. Moreover, tissue samples such as heart, lung, liver, spleen, bladder, kidneys and tumor were collected and split in two halfs: one fraction was put in an Eppendorf tube and stored at −80 °C for further quantification of DTX accumulation level by LC-MS analysis. The second half was fixed in 4 % paraformaldehyde in PBS overnight at 4 °C for the histological study.

Animal welfare was evaluated daily using the Morton and Griffiths scale and facial expressions (Langford et al., 2010; Morton and Griffiths, 1985; Scharmann, 1999).

2.4. Biodistribution study

Obtained plasma, tumor and tissue samples for determination of accumulated DTX were stored at −80 °C until use. Sample processing was carried out according to standard protocols (Zhao et al., 2010, 2011). In short, 100 mg of tumor or major organ tissue or 100 μL of plasma was mixed with 500 μL of PBS in a 2 mL lysing matrix D tube containing zirconium oxide spheres (MP Biomedicals, Santa Ana, CA, USA), and 20 μL of a paclitaxel (PTX) solution (10 μg/mL) was spiked as internal standard (Hendrikx et al., 2013; Lee et al., 2016; Rafiei et al., 2015). Then, the mixture was homogenized in a FastPrep-24TM instrument (MP Biomedicals). Organs underwent two cycles of homogenization (6 m/s during 40 s), except for the heart and tumor, which required six cycles. Then, 1 mL of diethyl ether (DEE) was added to the resulting homogenate, the suspension was transferred to a 2 mL Eppendorf tube and vortexed for 1 min, followed by centrifugation 10 min at 9,300 rcf. The organic phase was transferred to clean tubes and the extraction was repeated with 1 mL of DEE. Subsequently, the extracts were evaporated to dryness under nitrogen stream at 35 °C, the residue was reconstituted with 120 μL of methanol, and a 5 μL aliquot was injected into a LCMS apparatus (LCMS-8040 Triple Quadrupole LC-MS System, Shimadzu, Kyoto, Japan). Experimental details of the DTX analytical protocol by LC-MS are shown at the Supplementary Information. In addition, in case of plasma, tissue and blood samples from N1 group mice, we also analyzed silicon from the nanoparticles colocalizing with DTX in tumor and the different tissue by inductive couple plasma (ICP, Varian 715-ES).

2.5. Histopathological analysis

For histological evaluation of fixed tissues (4 % paraformaldehyde in PBS) from heart, lung, liver, spleen, bladder and kidneys as well as the tumor tissue, samples were dehydrated and placed into paraffin blocks using a Modular tissue embedding center (Myr, SL). Serial sections were cut of 7 μm thickness using an HM340E Electronic rotary microtome (VWR International, Barcelona, Spain). Rehydrated sections were stained with hematoxylin/eosin (H&E) in ST5010 Autostainer XL (Leica, Wetzlar, Germany) and scanned using an Aperio Versa scanner (Leica, Wetzlar, Germany) for further visual evaluation.

2.6. Immunohistochemistry

For the analysis of apoptosis/proliferation profile, sections embedded in paraffin were first heated at 65 °C for 30 min to remove excess paraffin, followed by rehydration and deparaffinization carried out in the Leica Autostainer. Next, antigen retrieval procedure was performed by incubating the sections for 20 min in Tris-EDTA Buffer (10 mM Tris Base, 1 mM EDTA Solution, 0.05 % Tween 20, pH 9) at 95 °C. Then, sections were blocked and permeabilized with a solution of 5 % donkey serum and 0.1 % Triton X-100 in PBS for 1 h at room temperature, incubated with primary antibody solution overnight in a humid chamber. Primary antibodies were employed using the following dilutions: mouse anti-Ki67 (1:200, Abcam, ab16667); or rabbit anti-Caspase 3 (1:200, Cell Signaling, 9662S). Conjugated secondary antibodies AlexaFluor 488 or 555 were used against the mouse and rabbit IgG primary antibodies, respectively, for 1 h at room temperature. Slides were counterstained with DAPI (1;1000, #D9542, Sigma) and mounted with Mowiol® (#81381, Sigma). Images from the histological analysis

were acquired from either Aperio Versa Scanner or Zeiss Apotome, visualized, and analyzed using Leica AperioScope and ImageJ.

2.7. Statistical analysis

The mean tumor volume and body weight, and corresponding SD were determined for each experiment, and results were presented as the mean ± SD. The statistical analysis of tumor volume and body weight data was performed with one-way analysis of variance and Tukey's *post-hoc* test, whilst DTX biodistribution data were compared by the Student's *t*-test. Significant differences among the groups were calculated at $p < 0.05$ or less. All the analysis and graphs were carried out by using GraphPad Prism 6 software (GraphPad Software, San Diego, CA, USA).

3. Results

3.1. Materials

We reported in a previous study the preparation of MNX nanoparticles (Rivero-Buceta et al., 2019). Firstly, the 2′-OH position of DTX was modified with succinic acid *via* an ester linkage to give the 2′-hemisuccinate docetaxel prodrug (Suc-DTX) (Liu et al., 2013). This way, the hydroxyl group of DTX is transformed into a more reactive terminal group, which binds more readily to the surface of silica nanoparticles functionalized with amino groups. Confirmation of the chemical structure was performed by NMR (^{1}H and ^{13}C) and UPLC-MS. The synthetic protocol and the characterization of the prodrug are described in the Supplementary Information (Scheme 1).

In parallel, MSNs were synthesized following a standard process and then grafted with amino groups on the surface by APTMS (3-aminopropyl)trimethoxysilane (MSN-NH_2). In the last step, the DTX prodrug was attached to the amino groups of the MSNs by amide bond.

The morphology and microstructure of the starting MSNs were investigated by Transmission Electron Microscopy (TEM) analysis (Fig. 1). All MSNs showed spherical shape and uniform particle size with very little polydispersity, and average diameter of 159 ± 23 nm. However, particle diameter calculated by DLS was always a little bit larger

Table 1
Different animal groups receiving DTX or MNX treatment considered in this study.[1.]

Administration route	Group	Dosage	Code	n
Intratumoral (IT)	Control	Vehicle	C1	5
	DTX	2 mg kg^{-1} DTX	D1	5
	DTX	10 mg kg^{-1} DTX	D2	5
	MNX	2 mg kg^{-1} DTX (equivalent)	N1	5
Intravenous (IV)	Control	Vehicle	C2	5
	DTX	2 mg kg^{-1}	D3	5

[1] Number of mice per group.

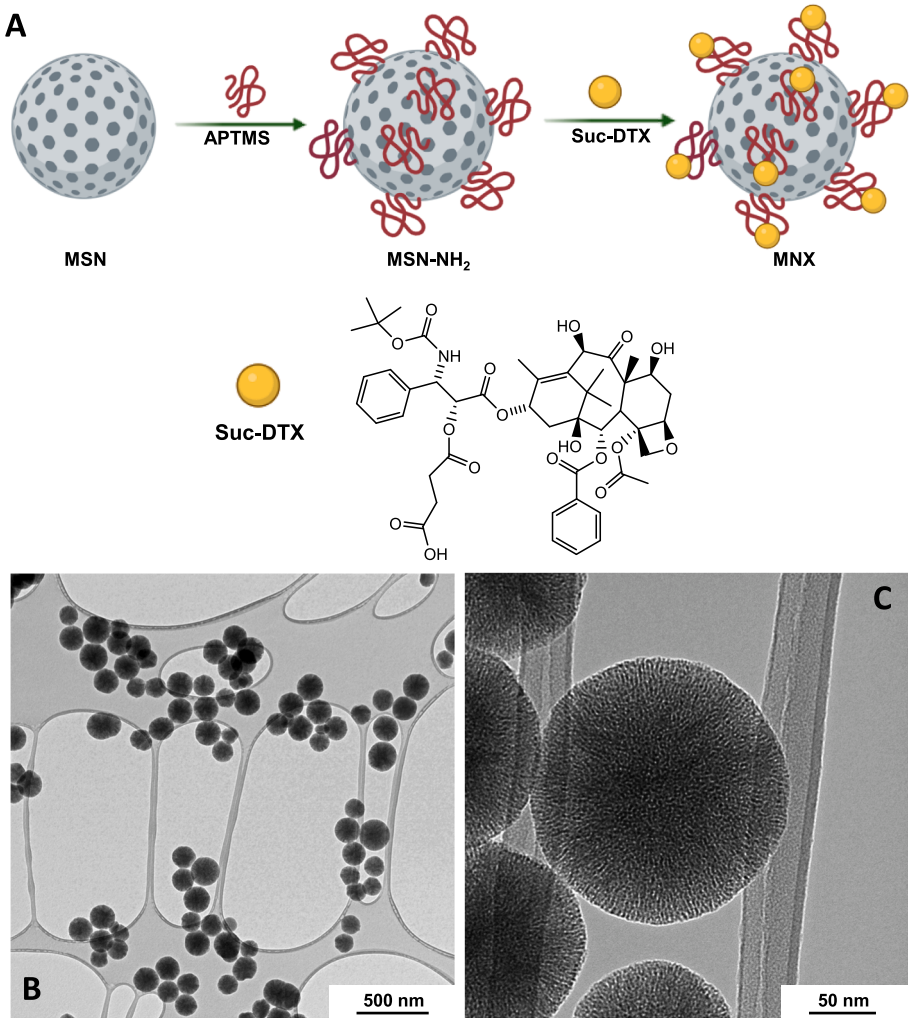

Fig. 1. MNX nanoparticles layout. (A) Artistic scheme of nanoparticles functionalization, also showing the 2′-hemisuccinate docetaxel structure (Suc-DTX). (B) As-prepared monodispersed MNX nanoparticles. (C) Mesoporous structure in MNX nanoparticles.

Table 2
Main variables monitored in the toxicity study over different animal groups receiving DTX or MNX treatment according to Morton & Griffiths test score (Morton and Griffiths, 1985).[1]

	IT Administration				IV Administration	
Experimental group	C1	D1	D2	N1	C2	D3
T/C ratio body weight (%)	0	8.69	5.39	16.01	0	−0.97
Pain	−	−	+	−	−	−
Ulceration	−	−	++	−	−	−
Impracticable veins	−	−	−	−	+	+
Tail necrosis/loss	−	−	−	−	−	−
Hematuria	−	−	−	−	−	−
Diarrhoea	−	−	−	−	−	−

[1] Mice incidence: +++≡100%; ++≡50%; +≡25%; −≡0%.

than that measured by TEM. This has been observed in many other nanoparticle systems (Rivero-Buceta et al., 2023), and it is due to somewhat nanoparticle aggregation in aqueous media, giving a few dimers and oligomers in the suspension, which increases to some extent the hydrodynamic diameter. In this context, we observed no relevant changes in particle diameter from the unmodified MSN-OH, the APTMS functionalized MSN-NH_2, and the final DTX-loaded material (see Table S1). The powder X-ray diffraction (XRD) measurement of MNXs showed the typical pattern of a nanoscale MCM-41 phase (Fig. S1B). Consistently, N_2 adsorption isotherms of MNXs matched a type IV isotherm (Fig. S1C).

These nanoparticles exhibited a BET specific surface area of 360 $m^2 g^{-1}$ (Barrett et al., 1951), a pore volume of 0.14 $cm^3 g^{-1}$, and a pore diameter of 3.0 nm (Kruk et al., 1997). However, it must be noted that the different functionalization steps provoke partial pore collapse, reducing drastically surface area and pore volume with regards the pristine material (See Table S1). In our case, the Zeta potential measurement was −7.4 mV after DTX incorporation. DTX loading content of the nanoparticles was also quantified by elemental analysis, showing DTX loading was 10.5–12 wt% (0.13–0.15 mmol g^{-1}). Eventually, DTX loading efficiency (as calculated by Eq. (2)) was 18–20 %.

3.2. Animals wellness. Morton and Griffiths test

The different groups of animals in the study are summarized in Table 1. To ensure the welfare of the animals, weight, pain and discomfort were monitored throughout the experiment following the method of Morton and Griffiths (Morton and Griffiths, 1985). Table 2 shows the essential variables supervised in this study in all treated and untreated groups in IT and IV administration. Overall, the weight of the animals remained stable during treatment in the different groups, regardless of the administration route. It is important to note that in no case did the animals suffer a weight loss of more than 20 % of their initial weight after a 16 days of treatment. All IT groups demonstrated a positive T/C body weight ratio (Table 2), which was notably higher in the nanoparticle group, indicating minimal systemic toxicity associated with the different treatments administered at the prescribed dose (Fig. S2).

However, T/C ratio of body weight (%) of animals in group D3 was −0.97 (Table 2), despite the low dose of docetaxel (2 mg kg^{-1}), which is an indicator of potential systemic toxicity in this treatment. IT administration of DTX at a dose of 2 mg kg^{-1} (groups D1 and N1) did not induce pain, and no damage and/or ulceration were observed. In contrast, ulceration at tumor site was detected in animals receiving 10 mg kg^{-1} of free DTX (group D2). After last dosage, two of five animals in this group had small tumor ulceration, and one of these was sacrificed after receiving 4 doses due to tumor ulceration and did not complete the treatment. None of the mice that received IT administration showed any symptoms of distress or changes in feeding, grooming, activity, posture or appearance.

With regard to IV administration, all doses were administered through the lateral tail vein. In some animals, the tail was moderately damaged at the administration point at the last dose or the last two doses. However, neither of the animals presented serious toxicity problems, nor necrosis or tail loss occurred. Furthermore, neither severe signs of pain were identified, nor the mice showed changes in feeding, grooming, activity or physical status. It should be noted that none of the groups presented symptoms such as hematuria or diarrhea.

3.3. Tumor evolution in IT and IV administration of DTX and MNX nanomedicine

LNCaP tumor-bearing mice were selected as the animal model to evaluate the antitumor effects of free DTX and MNX. These agents were administered *via* IT and compared to IV injection of DTX. Both treatment routes involved administration every 4 days over a total duration of 16 days. As shown in Fig. 2A, IT treatments significantly inhibited tumor growth compared to the control group ($p < 0.01$), irrespective of the administered DTX dose (2 mg kg^{-1} or 10 mg kg^{-1}). Conversely, IV administration of DTX did not demonstrate potential to reduce tumor volume at the lower dose (2 mg kg^{-1}) (Fig. 3A). In addition, no significant macroscopic modifications to the major organs (spleen, kidneys, liver) were detected in any of the treatment groups (Fig. 2B, Fig. 3B).

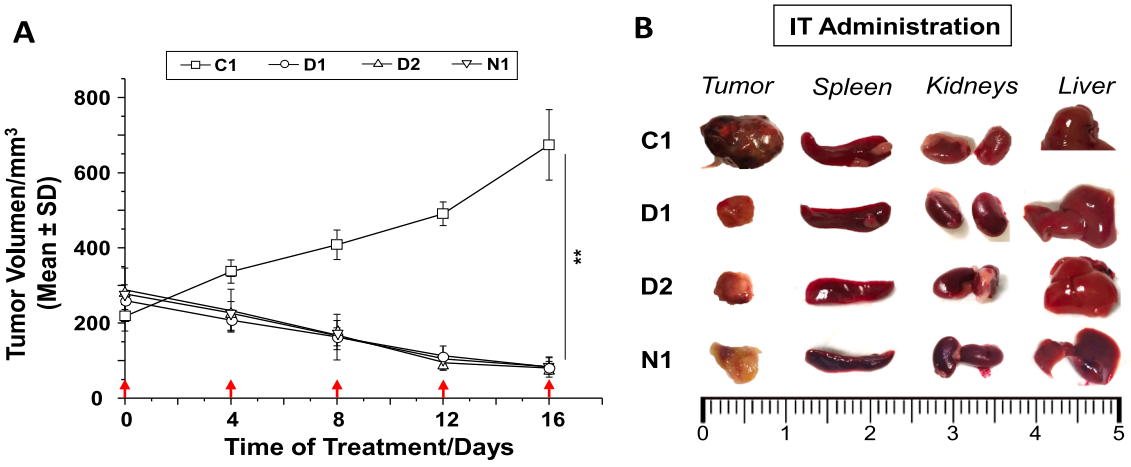

Fig. 2. Tumor suppression study in IT administration. (A) Analysis of the localized s.c. growth of the LNCaP prostate cancer tumor in groups of athymic nude mouse administered IT with vehicle (C1), DTX (D1: 2 mg kg^{-1}, D2: 10 mg kg^{-1}) or MNX nanomedicine (N1: 2 mg kg^{-1} DTX equivalent). Arrows indicate dosing time. (B) Size and appearance of tumor and major organs after therapy by IT administration. Arrows indicate treatment time. $^{**}p < 0.01$.

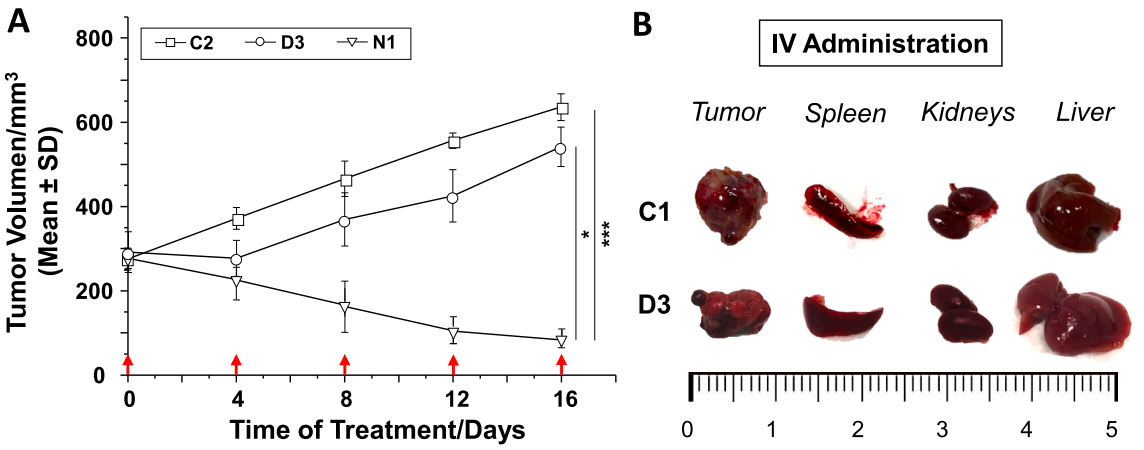

Fig. 3. Tumor suppression study in IV administration. (A) Analysis of the localized s.c. growth of the LNCaP prostate cancer tumor in groups of athymic nude mouse administered IV with vehicle (C2) or DTX (D3: 2 mg kg^{-1}). N1 group data (IT administration of MNX nanomedicine) is comparatively introduced. Arrows indicate treatment time. (B) Size and appearance of tumor and major organs after therapy by IV administration. *$p < 0.05$; ***$p < 0.001$.

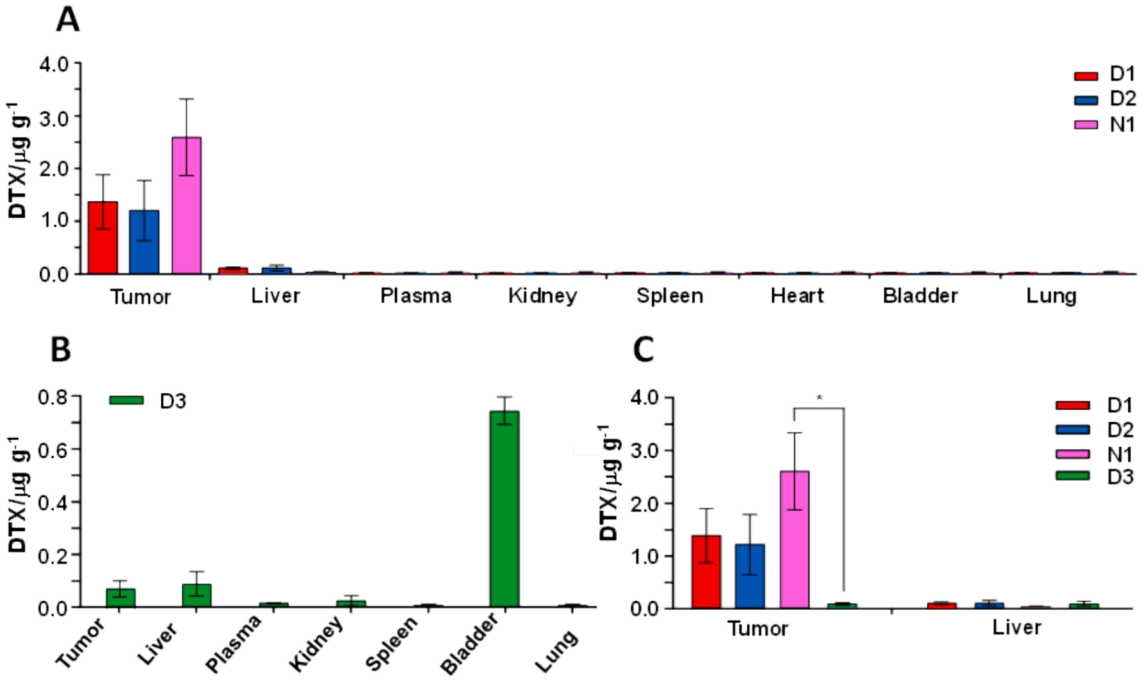

Fig. 4. DTX biodistribution. (A) Level quantification in *ex vivo* tumor and tissue samples after IT administration in athymic nude mice of DTX (D1: 2 mg kg^{-1}, D2: 10 mg kg^{-1}) or MNX nanomedicine (N1: 2 mg kg^{-1} DTX equivalent). (B) Level quantification in *ex vivo* tumor and tissue samples after IV administration in athymic nude mice of DTX (D3: 2 mg kg^{-1}). (C) Comparative study of tumor and liver DTX levels after IT/IV administration. *$p < 0.05$.

In any case, we have to take into account that these results have been obtained over a mouse model of subcutaneous tumor. In this context, it has been described that PCa subcutaneous tumors have significantly lower levels of perfusion than orthotopic tumors, and higher levels of hypoxia levels (Zhang et al., 2019). Consequently, it is expectable that the tumor growth inhibition activity observed after IT administration could be even stronger in case of orthotopic implants.

3.4. Biodistribution study

To examine *in vivo* drug release, docetaxel biodistribution in major organs was evaluated in athymic nude mice bearing the LNCaP tumor 24 h after the latest injection by comparing groups receiving IT or IV treatment. Levels of DTX present in plasma, liver, spleen, kidney, lung, bladder, heart, and tumor tissues were quantified through LCMS analysis (see protocols at the Supplementary Information, Table S3, Fig. S3 and Fig. S4).

Fig. 4A illustrates the specific biodistribution evaluation in organs following IT treatments. The results indicate that DTX primarily accumulates within the tumor when administered directly.

Whilst the administration of free DTX leads to comparable accumulation in tumor irrespective of the dosage (2 mg kg^{-1} or 10 mg kg^{-1}), a notable increase was observed when delivered by MNX (2 mg kg^{-1} of equivalent DTX). Although differences were not significant from a statistical point of view ($p = 0.052$), it is clear the preferential accumulation of DTX in tumor when administering the nanomedicine. Additionally, DTX was detected in liver when administered in its free form, but not when injecting the nanomedicine. Notably, 24 h after injection, no DTX was observed in any other organ.

Conversely, IV administration of DTX (2 mg kg^{-1}) was subjected to

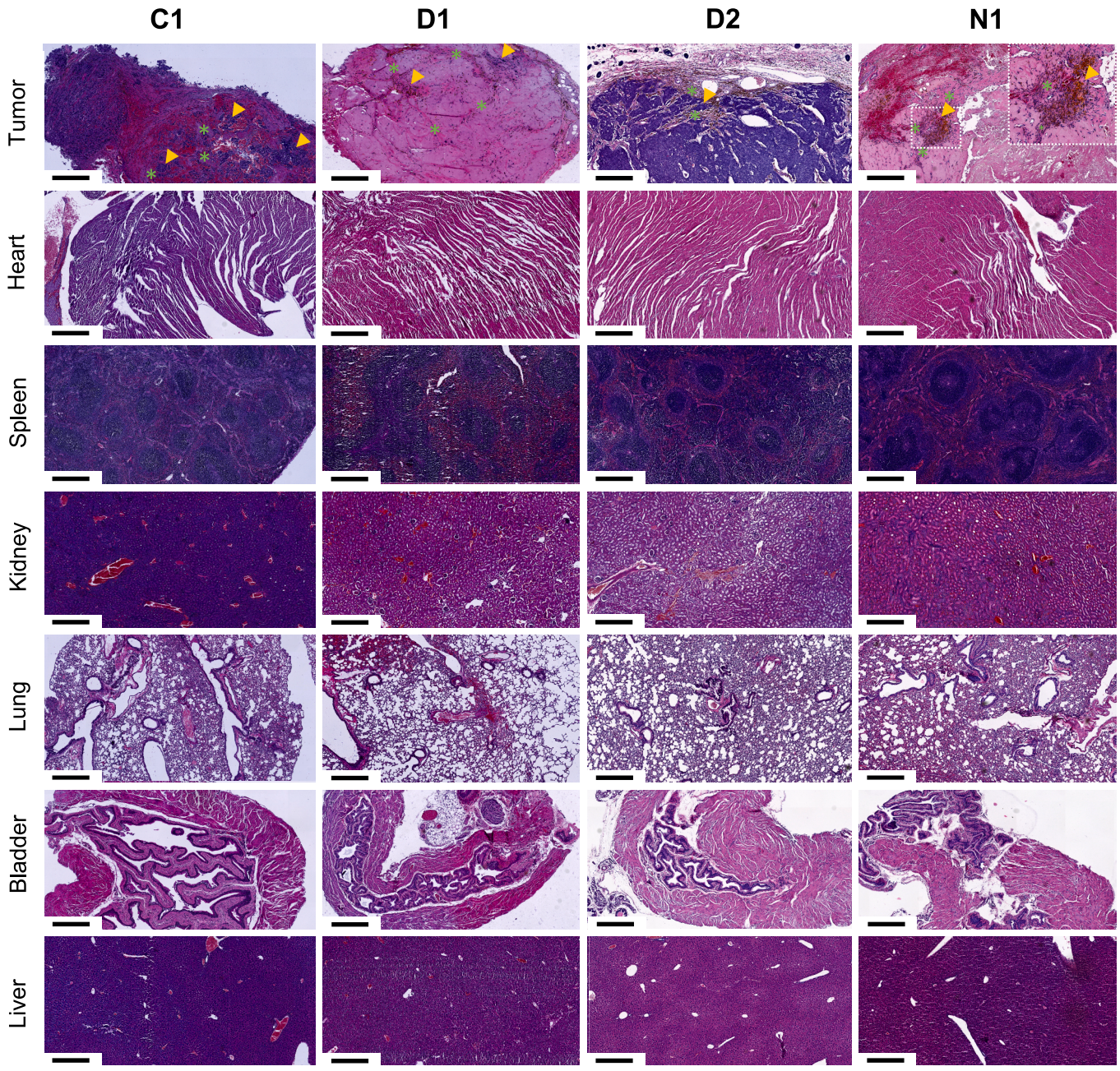

Fig. 5. Hematoxylin/eosin staining of histological sections after end point of athymic nude mice administered IT with vehicle (C1), DTX (D1: 2 mg kg^{-1}, D2: 10 mg kg^{-1}) or MNX nanomedicine (N1: 2 mg kg^{-1} DTX equivalent). Yellow arrows mark tumor cells grouped in concentric clusters surrounded by extracellular matrix fibroblast-like infiltrating cells (green dots*). The inset in Tumor/N1 slice shows the magnification of a cluster of tumor cells. Scale bar: 700 μm. (For interpretation of the references to colour in this figure legend, the reader is referred to the web version of this article.)

quick plasma clearance, promoting accumulation mostly in bladder, with low levels detected in plasma, kidneys, liver and tumor (Fig. 4B). Indeed, the comparison between tumor DTX stock by IT administration of the nanomedicine (N1 group) *vs* IV injection of the free drug (D3 group) at same drug dosage (2 mg kg^{-1}) reported significant differences ($p < 0.05$) (Fig. 4C).

In case of N1 group, we also tried to determine silicon from the nanoparticles colocalizing with DTX in tumor and the different tissue by inductive couple plasma (ICP) analysis. Here, Si concentration in tumor was clearly detected (18.2 μg/g), which is consistent with the quantified DTX. However, due to the low dosage level implemented, Si content in the different organs analyzed was below the sensitivity of the technique (Aureli et al., 2020).

3.5. Histopathological study and immunohistochemistry

At the endpoint, the tumor volume was significantly reduced in the treated groups in comparison with the corresponding controls, in agreement with their lower cellularity found in the Hematoxylin/eosin staining's shown in Fig. 5 and Fig. 6, demonstrating the efficacy of the treatments targeting the tumoral cells. At this late stage, the dead tumoral cells after pharmacological treatments were already phagocyte/clean-up.

The pathological study of tumor slices in control groups, either from IT or IV vehicle administration, showed compact tumor cell aggregation with no cavities and no necrotic areas (Fig. 5, C1 group; Fig. 6, C2 group). The tumor cells were grouped in cluster (yellow arrows),

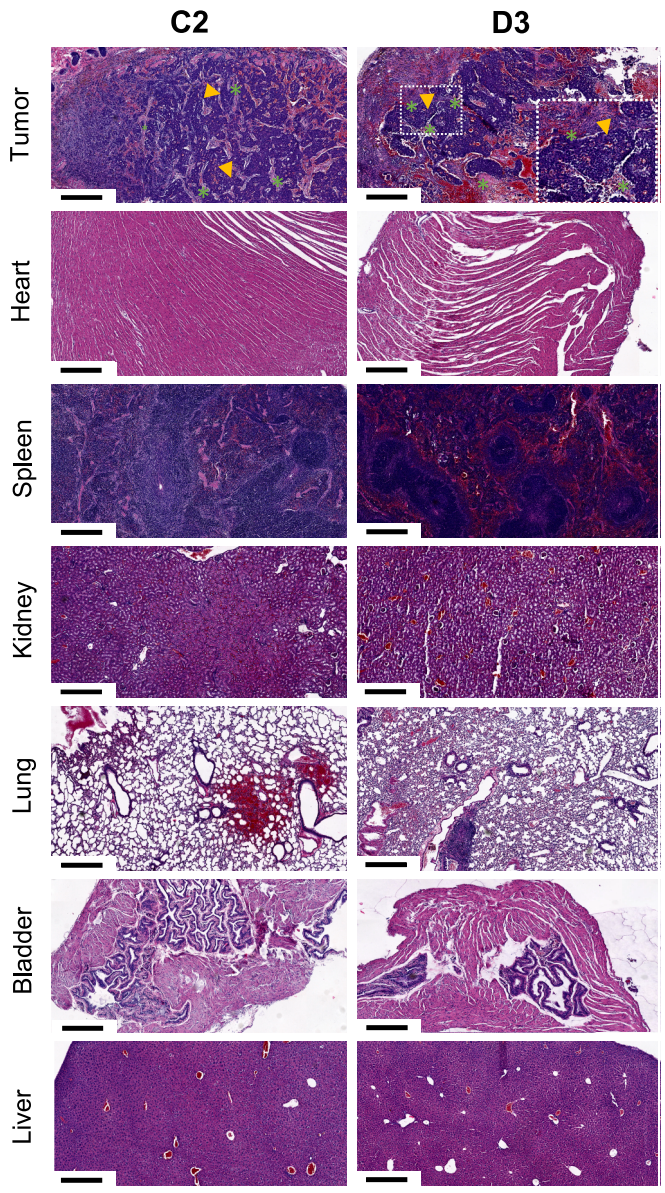

Fig. 6. Hematoxylin/eosin staining of histological sections after end point of athymic nude mice administered IV with vehicle (C2) or DTX (D3: 2 mg kg^{-1}). Yellow arrows mark tumor cells grouped in concentric clusters surrounded by extracellular matrix fibroblast-like infiltrating cells (green dots*). The inset in Tumor/D3 slice shows the magnification of a cluster of tumor cells. Scale bar: 700 μm. (For interpretation of the references to colour in this figure legend, the reader is referred to the web version of this article.)

frequently found in concentrically organization surrounded by extracellular matrix and infiltrated fibroblast-like cells (green dots*). Abundant blood red vessels invading both, fibrotic and tumor areas were found indicating a highly vascularized tumor formation.

However, the IT administration of DTX at concentration of 2 mg kg^{-1} showed a significant lower number of tumor cells with regards its corresponding control sample. Dispersed tumor cells with few small and diffused cell clusters were embedded by a dense extracellular matrix. Limited vascularization, no oedema, no cavities and no necrotic areas were evidenced (Fig. 5, D1 group). No improvement was observed when administering DTX at concentration of 10 mg kg^{-1} (Fig. 5, D2 group). Then, the IT administration of MNX at concentration of 2 mg kg^{-1} equivalent DTX showed significant lower number of tumor cells when comparing with the corresponding control group. Here, few clusters of tumor cells dispersed and concentrically organized were surrounded by abundant fibrotic tissue and extracellular matrix, encapsulated by a thick envelop of matrix. Very poor vascularization and no oedema were present (Fig. 5, N1 group). In addition, immunodetection of Ki67 (in green, white arrows), a mitotic marker, and Caspase 3 (in red, red arrows), a pro-apoptotic marker, and counterstaining of nuclei with DAPI (blue) also evidenced a reduction in the number of proliferating cells (green) and an increased number of dying cells (red) in all treated groups compared with the control condition (Fig. 7).

Conversely, the tumor formation after IV administration of DTX at 2 mg kg^{-1} showed compact and dense tumor cell clusters, with trabecula-like formations surrounded by fibrotic tissue driving abundant blood vessels at the core of the tumor (Fig. 6, D3 group).

No pathological processes were found or evidenced in any of the peripheral evaluated organs (heart, spleen, kidney, lung, bladder and liver) for any of the treatments. No necrotic signs, no sclerosis, no oedema, no hypertrophic signs, no abnormal cell organization, and no tumor formation signs were detected (Figs. 5 and 6).

4. Discussion

Prostate cancer is common in older men (median age 68) and diagnoses in men > 65 will result in a 70 % increase in annual diagnosis by 2030 in Europe and the USA (Arnold et al., 2015; Smith et al., 2009). Older men may be under-treated due to secondary effects of current local disposable treatments as surgery or radiotherapy for localized and locally advanced.

In this study, we provide a detailed description of efficacy, tolerability, biodistribution and histopathology following IT administration of DTX and MSN nanomedicines in athymic nude male mice bearing human prostate adenocarcinoma tumors. Additionally, these results were compared with IV administration of DTX.

In the field of current cancer treatment strategies, two notable areas are emerging: i) the exploration of new administration routes such as local treatment of solid tumors to address the limitations of conventional IV chemotherapy (Brachi et al., 2020; Ginat et al., 2022; Liu et al., 2022), and ii) the use of drug delivery systems to enhance and minimize systemic toxicity, overcoming the pharmacoresistance exhibited by some chemotherapeutic agents (Corma et al., 2022; Jackson et al., 2023; Qu et al., 2016). At this point, nanoscale systems show an excellent profile for local delivery of therapeutic agents. It must be taken into account that the successful diffusion of drugs involves an efficient penetration through the tumor microenviroment, which is strongly hampered for large particle diameters, like microspheres, which are readily trapped by the extracellular matrix, precluding their entrance in interstitial tumor spaces (Ding et al., 2019). Furthermore, another promising DDSs are the *in situ* forming gels, which can be injected as a liquid and the solution turns into a depot only upon administration (Pandya et al., 2023). For this purpose, a specific and timed trigger is compulsory, such as temperature, pH, ionic change or specific molecular cues present in the tumor microenviroment. At this point, it is remarkable the commercial OncoGel®, a thermosensitive hydrogel formulation of paclitaxel that has shown ability to improve current treatment options in superficially-palpable tumors and esophageal carcinoma, and could have a chance against PCa (Tanga et al., 2023).

Here, mesoporous silica nanoparticles (MSN) were selected as DDS due to their attractive properties, namely large surface areas, tunable pore sizes, and good biocompatibility. We have previously developed MSN loaded with DTX, which demonstrated greater cytotoxicity with regard to free DTX in LNCaP cells (Rivero-Buceta et al., 2019). These covalent conjugations prevent the drug from releasing prematurely before reaching the tumor site (Wang et al., 2020). By this protocol DTX was incorporated at 10.5–12 wt% on the surface of the nanoparticles. Additionally, the functionalization of the nanoparticles with amino groups aimed to decrease their inherent tendency to aggregate, thereby enhancing their biodistribution and cellular uptake (Bagwe et al., 2006;

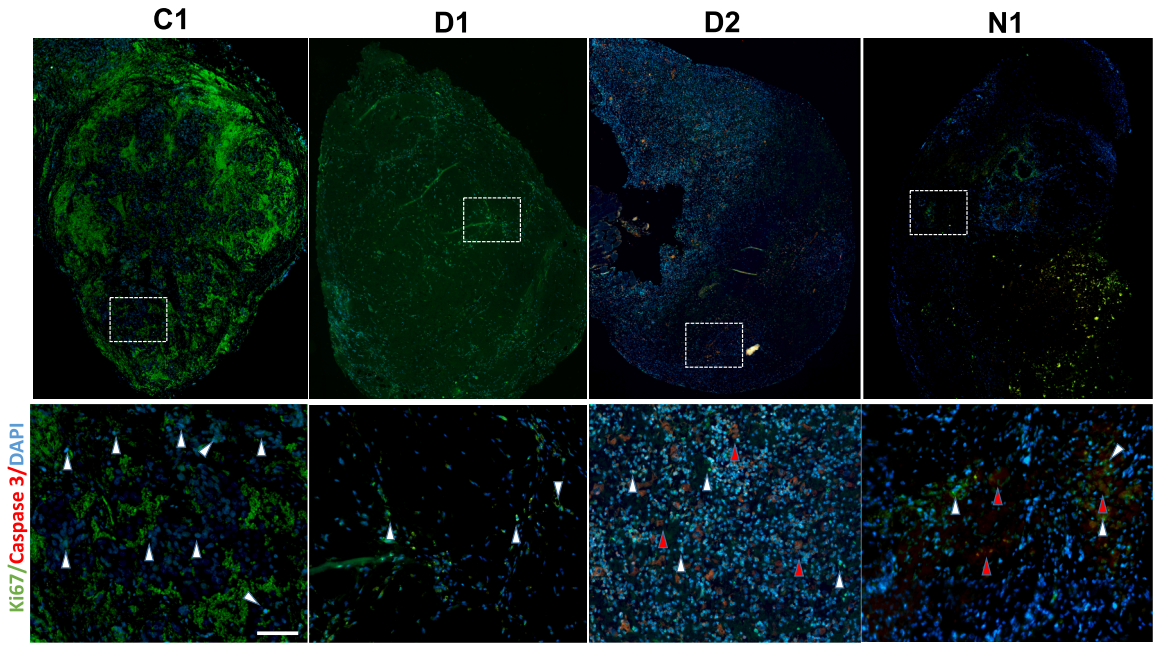

Fig. 7. Immunohistochemical study for Ki67 and Caspase 3 of slices after end point of athymic nude mice administered IT with vehicle (C1), DTX (D1: 2 mg kg-1, D2: 10 mg kg-1) or MNX nanomedicine (N1: 2 mg kg-1 DTX equivalent). Top panels: Panoramic view of tumor tissue; Bottom panels: Magnification of the area of the white dotted square (scale bar: 300 μm). Ki67 green, white arrows; Caspase 3 red, red arrows. (For interpretation of the references to colour in this figure legend, the reader is referred to the web version of this article.)

Estevão et al., 2021).

In recent years, much attention has been directed toward IT administration due to several advantages, such as higher drug accumulation in tumor tissue and lower systemic toxicity (Brachi et al., 2020; Maulhardt et al., 2019; Yun et al., 2023). Moreover, immune response, opsonization and plasma clearance are important issues related with the IV administration of nanoparticle based DDSs, which would be strongly minimized by IT administration (Clemments et al., 2014). The size and properties of nanoparticles, the tumor environment and the administration process, including speed, dosage and site, are aspects that must be considered when developing nanoparticles for administration through this route. These aspects directly influence the dispersion of the suspension at the tumor site and its clearance, thereby impacting its therapeutic efficacy (Yun et al., 2023).

Monitoring tumor volume allowed for the evaluation of the antitumor effectiveness of both IT and IV DTX, as well as IT administered nanoparticles. Our results demonstrated that IT administration of mice with free DTX at different doses (2 mg kg^{-1} and 10 mg kg^{-1}) and with DTX-loaded MSN, show comparable tumor shrinkage. No weight loss was noted in animals, indicating no potential toxicity of the treatment. However, it must be taken into account that the higher IT dose of DTX resulted in ulceration in the tumor region in some animals, which recommends to work at low dosage profile.

The biodistribution study showed that DTX nanomedicine administered by IT route allowed higher drug retention within the tumor. Indeed, in case of IT injection of the single therapeutic molecule it was also detected in liver (undetectable for the nanoparticle DDS). This suggests that MSN serve as an efficient DTX carrier system, promoting controlled release in tumor tissue, as already described for other nanoparticles (Yu et al., 2019). At this point, our nanomedicine presents optimized characteristics that enhance tumor penetration and diffusion, as small size (Dp $<$ 200 nm), spheroid shape and moderately negative charge (Z∼-7 mV) (Ding et al., 2019).

Furthermore, the covalent linkage of DTX on MSN nanoparticles contributes to sustaining drug levels within the tumor over the course of treatment, resulting in monitored drug release at the tumor site. With regard to the time scale of ester hydrolysis, we recently demonstrated in an *in vitro* study (Rivero-Buceta et al., 2019) that nanoparticles colocalized with acidic compartments labeled by LysoTracker after 24 h incubation with LNCaP cells, and significant cell viability reduction was found after 72 h incubation of cells with MNX nanoparticles. In this case, DTX discharge takes place by cell internalization via clathrin-mediated endocytosis and later cytosolic carboxylases activity, degrading ester bonds (Botella et al., 2011). In addition, nanoparticles not only increase the drug concentration at the tumor site, but also minimize systemic diffusion of DTX. Moreover, the application of nanomedicines in IT delivery aims to prevent the rapid plasma clearance and elimination of drugs from tumor tissue into the bloodstream and in the vicinity of normal tissues by regulating their diffusion (Brachi et al., 2020).

Once the optimized IT dose (2 mg kg^{-1}) was established, free DTX was IV administered at this same dose to compare results. However, this IV dosage is one order below the standard therapeutic dosing needed by this route, and no effect over tumor growth was observed (Naguib et al., 2014; Tang et al., 2016). In this context, after IV administration of soluble DTX, the accumulation in different organs, but specially bladder, was noticeable, whereas less than 1 % of the initial dose was confined in tumor. At this point, even when administering *via* IV DTX nanomedicines, which are expected to favor drug accumulation in tumor by enhanced permeability retention (EPR) effect, the IV administration needs of a dose range over 20 mg kg^{-1} of DTX in order to achieve a therapeutic outcome (Li et al., 2010; Poltavets et al., 2019).

In addition, the animals in this group experienced an important weight loss throughout the treatment, indicating systemic toxicity. Finally, the H&E showed no pathological processes in major organs for all groups. However, in the groups displaying an antitumor effect, significant reduction in the number of tumor cells was observed within specific areas.

5. Conclusions

We have proven in a xenograft mice model of human prostate adenocarcinoma that IT injection of DTX MSN-based nanomedicines allow performing precise and selective therapy of non-metastatic PCa with higher drug accumulation at the tumor site and lower systemic

diffusion. Indeed, IT administration of DTX has shown superior activity than IV route in PCa therapy, allowing reduction of the therapeutic dose by one order, and widening substantially the therapeutic window for this drug. In this context, DTX nanomedicine has shown the same antitumor activity than the free drug by IT route. Moreover, the use of DTX nanomedicines in combination with IT injection promotes strong antitumor efficacy and drug accumulation at the tumor site, improving the results obtained with the free drug. Albeit further exploration is required regarding the efficacy of this treatment in orthotopic tumors, as well as long-term toxicity studies of these nanomedicines under IT administration, this represents an effective therapeutic protocol for PCa therapy.

6. Institutional Review Board Statement

The study was conducted in accordance with the Declaration of Helsinki, and approved by the Ethics Committee of Instituto de Investigación Sanitaria La Fe (protocol code 2019-024-1; date of approval: 2019-10-30).

Funding

Financial support by the Spanish National Research Agency [PID2022142952OB-100 grant], Generalitat Valenciana [CIPROM/2021/003 grant] and the Spanish Ministry of Science and Innovation (CEX2021-001230-S grant funded by MCIN/AEI/10.13039/501100011033) is gratefully acknowledged.

CRediT authorship contribution statement

Eva Rivero-Buceta: Writing – original draft, Visualization, Validation, Investigation, Formal analysis. **Adrián Bernal-Gómez:** Visualization, Validation, Investigation, Formal analysis. **Carla Vidaurre-Agut:** Investigation. **Eric Lopez Moncholi:** Visualization, Validation, Investigation. **Jose María Benlloch:** Writing – review & editing, Project administration, Methodology, Funding acquisition. **Victoria Moreno Manzano:** Writing – review & editing, Writing – original draft, Visualization, Validation, Methodology, Investigation, Formal analysis. **César David Vera Donoso:** Writing – review & editing, Supervision, Project administration, Methodology, Conceptualization. **Pablo Botella:** Writing – review & editing, Writing – original draft, Supervision, Project administration, Methodology, Funding acquisition, Conceptualization.

Declaration of competing interest

The authors declare the following financial interests/personal relationships which may be considered as potential competing interests: [Pablo Botella Asuncion reports financial support was provided by State Agency of Research. Pablo Botella Asuncion reports financial support was provided by Government of Valencia. Pablo Botella Asuncion has patent #WO2021/099662 issued to Universitat Politècnica de Valencia-Consejo Superior de Investigaciones Cientificas. If there are other authors, they declare that they have no known competing financial interests or personal relationships that could have appeared to influence the work reported in this paper.].

Data availability

Data will be made available on request.

Acknowledgements

The authors thank Dr. Viviana Bisbal Velasco, Dr. Delia Castellano Izquierdo and Ms. Nerea Martín Izquierdo for their help and support in the in vivo experiments.

Appendix A. Supplementary material

Synthetic protocols of DTX prodrug and nanomedicine. Characterization reports of DTX nanomedicine. In vivo testing data: DTX administration, T/C ratios, body weight curves, DTX analysis in biological samples by LCMS. Supplementary data to this article can be found online at https://doi.org/10.1016/j.ijpharm.2024.124623.

References

Arnold, M., Karim-Kos, H.E., Coebergh, J.W., Byrnes, G., Antilla, A., Ferlay, J., Renehan, A.G., Forman, D., Soerjomataram, I., 2015. Recent trends in incidence of five common cancers in 26 European countries since 1988: Analysis of the European Cancer Observatory. Eur. J. Cancer 51, 1164–1187. https://doi.org/10.1016/j.ejca.2013.09.002.

Aureli, F., Ciprotti, M., D'amato, M., da Silva, E.D.N., Nisi, S., Passeri, D., Sorbo, A., Raggi, A., Rossi, M., Cubadda, F., 2020. Determination of total silicon and SiO2 particles using an ICP-MS based analytical platform for toxicokinetic studies of synthetic amorphous silica. Nanomaterials 10. https://doi.org/10.3390/nano10050888.

Bagwe, R.P., Hilliard, L.R., Tan, W., 2006. Surface modification of silica nanoparticles to reduce aggregation and nonspecific binding. Langmuir 22, 4357–4362. https://doi.org/10.1021/la052797j.

Barrett, E.P., Joyner, L.G., Halen, 1951. The Determination of Pore Volume and Area Distributions in Porous Substances. I. Computations from Nitrogen Isotherms. J. Am. Chem. Soc. 73, 373–380. https://doi.org/10.1021/ja01145a126.

Bobo, D., Robinson, K.J., Islam, J., Thurecht, K.J., Corrie, S.R., 2016. Nanoparticle-Based Medicines: A Review of FDA-Approved Materials and Clinical Trials to Date. Pharm. Res. 33, 2373–2387. https://doi.org/10.1007/s11095-016-1958-5.

Botella, P., Abasolo, I., Fernández, Y., Muniesa, C., Miranda, S., Quesada, M., Ruiz, J., Schwartz, S., Corma, A., 2011. Surface-modified silica nanoparticles for tumor-targeted delivery of camptothecin and its biological evaluation. J. Control. Release 156, 246–257. https://doi.org/10.1016/j.jconrel.2011.06.039.

Brachi, G., Ruiz-Ramírez, J., Dogra, P., Wang, Z., Cristini, V., Ciardelli, G., Rostomily, R. C., Ferrari, M., Mikheev, A.M., Blanco, E., Mattu, C., 2020. Intratumoral injection of hydrogel-embedded nanoparticles enhances retention in glioblastoma. Nanoscale 12, 23838–23850. https://doi.org/10.1039/d0nr05053a.

Cai, Q., Luo, Z.S., Pang, W.Q., Fan, Y.W., Chen, X.H., Cui, F.Z., 2001. Dilute solution routes to various controllable morphologies of MCM-41 silica with a basic medium. Chem. Mater. 13, 258–263. https://doi.org/10.1021/cm990661z.

Cavallaro, P.A., De Santo, M., Belsito, E.L., Longobucco, C., Curcio, M., Morelli, C., Pasqua, L., Leggio, A., 2023. Peptides Targeting HER2-Positive Breast Cancer Cells and Applications in Tumor Imaging and Delivery of Chemotherapeutics. Nanomaterials. https://doi.org/10.3390/nano13172476.

Celikoglu, F., Celikoglu, S.I., Goldberg, E.P., 2008. Bronchoscopic intratumoral chemotherapy of lung cancer. Lung Cancer. https://doi.org/10.1016/j.lungcan.2008.03.009.

Clemments, A.M., Muniesa, C., Landry, C.C., Botella, P., 2014. Effect of surface properties in protein corona development on mesoporous silica nanoparticles. RSC Adv. 4, 29134–29138. https://doi.org/10.1039/c4ra03277b.

Corma, A., Botella, P., Rivero-Buceta, E., 2022. Silica-Based Stimuli-Responsive Systems for Antitumor Drug Delivery and Controlled Release. Pharmaceutics 14. https://doi.org/10.3390/pharmaceutics14010110.

Crown, J., O'Leary, M., Ooi, W.-S., 2004. Docetaxel and Paclitaxel in the Treatment of Breast Cancer: A Review of Clinical Experience. Oncologist 9, 24–32. https://doi.org/10.1634/theoncologist.9-suppl_2-24.

Ding, J., Chen, J., Gao, L., Jiang, Z., Zhang, Y., Li, M., Xiao, Q., Lee, S.S., Chen, X., 2019. Engineered nanomedicines with enhanced tumor penetration. Nano Today 29, 100800. https://doi.org/10.1016/j.nantod.2019.100800.

Engels, F.K., Sparreboom, A., Mathot, R.A.A., Verweij, J., 2005. Potential for improvement of docetaxel-based chemotherapy: A pharmacological review. Br J Cancer 93, 173–177. https://doi.org/10.1038/sj.bjc.6602698.

Engels, F.K., Mathot, R.A.A., Verweij, J., 2007. Alternative drug formulations of docetaxel: A review. Anticancer Drugs 18, 95–103. https://doi.org/10.1097/CAD.0b013e3280113338.

Escriche-Navarro, B., Escudero, A., Lucena-Sánchez, E., Sancenón, F., García-Fernández, A., Martínez-Máñez, R., 2022. Mesoporous Silica Materials as an Emerging Tool for Cancer Immunotherapy. Adv. Sci. https://doi.org/10.1002/advs.202200756.

Estevão, B.M., Miletto, I., Hioka, N., Marchese, L., Gianotti, E., 2021. Mesoporous silica nanoparticles functionalized with amino groups for biomedical applications. ChemistryOpen 10, 1251–1259. https://doi.org/10.1002/open.202100227.

Ferlay, J., Soerjomataram, I., Dikshit, R., Eser, S., Mathers, C., Rebelo, M., Parkin, D.M., Forman, D., Bray, F., 2015. Cancer incidence and mortality worldwide: Sources, methods and major patterns in GLOBOCAN 2012. Int. J. Cancer 136, E359–E386. https://doi.org/10.1002/ijc.29210.

Geney, R., Ungureanu, I.M., Li, D., Ojima, I., 2002. Overcoming multidrug resistance in taxane chemotherapy. Clin. Chem. Lab. Med. 40, 918–925. https://doi.org/10.1515/CCLM.2002.161.

Ginat, D.T., Juloori, A., Vivar, O.I., Farber, L.A., Gooi, Z., Rosenberg, A.J., 2022. Imaging Features of Intratumoral Injection of NBTXR3 for Head and Neck Squamous Cell Carcinoma Lymph Node Metastases. Diagnostics 12. https://doi.org/10.3390/diagnostics12092156.

Goldberg, E.P., Hadba, A.R., Almond, B.A., Marotta, J.S., 2010. Intratumoral cancer chemotherapy and immunotherapy: opportunities for nonsystemic preoperative drug delivery. J. Pharm. Pharmacol. 54, 159–180. https://doi.org/10.1211/0022357021778268.

He, X., Wang, J., Li, Y., 2015. Efficacy and safety of docetaxel for advanced non-small-cell lung cancer: A meta-analysis of phase iii randomized controlled trials. Onco Targets Ther 8, 2023–2031. https://doi.org/10.2147/OTT.S85648.

Hendrikx, J.J.M.A., Dubbelman, A.C., Rosing, H., Schinkel, A.H., Schellens, J.H.M., Beijnen, J.H., 2013. Quantification of docetaxel and its metabolites in human plasma by liquid chromatography/tandem mass spectrometry. Rapid Commun. Mass Spectrom. 27, 1925–1934. https://doi.org/10.1002/rcm.6654.

Jackson, N., Hill, I., Alhussan, A., Bromma, K., Morgan, J., Abousaida, B., Zahra, Y., Mackeyev, Y., Beckham, W., Herchko, S., Krishnan, S., Chithrani, D.B., 2023. Dual enhancement in the radiosensitivity of prostate cancer through nanoparticles and chemotherapeutics. Cancer Nanotechnol. 14 https://doi.org/10.1186/s12645-023-00228-0.

Jiang, Z., Fu, Y., Shen, H., 2024. Development of Intratumoral Drug Delivery Based Strategies for Antitumor Therapy. Drug Des Devel Ther 18, 2189–2202. https://doi.org/10.2147/dddt.s467835.

Kaye, S.B., Piccart, M., Aapro, M., Kavanagh, J., 1995. Docetaxel in advanced ovarian cancer: preliminary results from three phase II trials. EORTC Early Clinical Trials Group and Clinical Screening Group, and the MD Anderson Cancer Center. Eur. J. Cancer 31A, S14–S17.

Kruk, M., Jaroniec, M., Sayari, A., 1997. Adsorption study of surface and structural properties of MCM-41 materials of different pore sizes. J. Phys. Chem. B 101, 583–589. https://doi.org/10.1021/jp962000k.

Langford, D.J., Bailey, A.L., Chanda, M.L., Clarke, S.E., Drummond, T.E., Echols, S., Glick, S., Ingrao, J., Klassen-Ross, T., Lacroix-Fralish, M.L., Matsumiya, L., Sorge, R. E., Sotocinal, S.G., Tabaka, J.M., Wong, D., Van Den Maagdenberg, A.M.J.M., Ferrari, M.D., Craig, K.D., Mogil, J.S., 2010. Coding of facial expressions of pain in the laboratory mouse. Nat. Methods 7, 447–449. https://doi.org/10.1038/nmeth.1455.

Lee, H.H., Hong, A., Cho, Y., Kim, S., Kim, W.J., Kim, H.I., 2016. Structural Characterization of Anticancer Drug Paclitaxel and Its Metabolites Using Ion Mobility Mass Spectrometry and Tandem Mass Spectrometry. J. Am. Soc. Mass Spectrom. 27, 329–338. https://doi.org/10.1007/s13361-015-1280-1.

Li, L., Tang, F., Liu, H., Liu, T., Hao, N., Chen, D., Teng, X., He, J., 2010. In vivo delivery of silica nanorattle encapsulated docetaxel for liver cancer therapy with low toxicity and high efficacy. ACS Nano 4, 6874–6882. https://doi.org/10.1021/nn100918a.

Liu, F., Feng, L., Zhang, L., Zhang, X., Zhang, N., 2013. Synthesis, characterization and antitumor evaluation of CMCS-DTX conjugates as novel delivery platform for docetaxel. Int. J. Pharm. 451, 41–49. https://doi.org/10.1016/j.ijpharm.2013.04.020.

Liu, J.Q., Zhang, C., Zhang, X., Yan, J., Zeng, C., Talebian, F., Lynch, K., Zhao, W., Hou, X., Du, S., Kang, D.D., Deng, B., McComb, D.W., Bai, X.F., Dong, Y., 2022. Intratumoral delivery of IL-12 and IL-27 mRNA using lipid nanoparticles for cancer immunotherapy. J. Control. Release 345, 306–313. https://doi.org/10.1016/j.jconrel.2022.03.021.

Maulhardt, H.A., Hylle, L., Frost, M.V., Tornio, A., Dafoe, S., Drummond, L., Quinn, D.I., Kamat, A.M., Dizerega, G.S., 2019. Local injection of submicron particle docetaxel is associated with tumor eradication, reduced systemic toxicity and an immunologic response in uro-oncologic xenografts. Cancers (basel) 11. https://doi.org/10.3390/cancers11040577.

Maulhardt, H., Marin, A., Hesseltine, H., diZerega, G., 2021. Submicron particle docetaxel intratumoral injection in combination with anti-mCTLA-4 into 4T1-Luc orthotopic implants reduces primary tumor and metastatic pulmonary lesions. Med. Oncol. 38, 1–13. https://doi.org/10.1007/s12032-021-01555-1.

Maulhardt, H., Verco, S., Baltezor, M., Marin, A., diZerega, G., 2023. Local administration of large surface area microparticle docetaxel to solid carcinomas induces direct cytotoxicity and immune-mediated tumoricidal effects: preclinical and clinical studies. Drug Deliv. Transl. Res. 13, 503–519. https://doi.org/10.1007/s13346-022-01226-2.

Mazzotta, E., De Santo, M., Lombardo, D., Leggio, A., Pasqua, L., 2022. Mesoporous silicas in materials engineering: Nanodevices for bionanotechnologies. Mater Today Bio. https://doi.org/10.1016/j.mtbio.2022.100472.

Mohan, A., Harris, K., Bowling, M.R., Brown, C., Hohenforst-Schmidt, W., 2018. Therapeutic bronchoscopy in the era of genotype directed lung cancer management. J. Thorac. Dis. https://doi.org/10.21037/jtd.2018.08.14.

Morton, D.B., Griffiths, P.H., 1985. Guidelines on the recognition of pain, distress and discomfort in experimental animals and an hypothesis for assessment. Vet. Rec. 116, 431–436. https://doi.org/10.1136/vr.116.16.431.

Naguib, Y.W., Rodriguez, B.L., Li, X., Hursting, S.D., Williams, R.O., Cui, Z., 2014. Solid lipid nanoparticle formulations of docetaxel prepared with high melting point triglycerides: In vitro and in vivo evaluation. Mol. Pharm. 11, 1239–1249. https://doi.org/10.1021/mp4006968.

Pandya, A.K., Vora, L.K., Umeyor, C., Surve, D., Patel, A., Biswas, S., Patel, K., Patravale, V.B., 2023. Polymeric in situ forming depots for long-acting drug delivery systems. Adv. Drug Deliv. Rev. https://doi.org/10.1016/j.addr.2023.115003.

Petrylak, D.P., 2006. The treatment of hormone-refractory prostate cancer: docetaxel and beyond. Rev. Urol. 8, S48–S55.

Poltavets, Y.I., Zhirnik, A.S., Zavarzina, V.V., Semochkina, Y.P., Shuvatova, V.G., Krasheninnikova, A.A., Aleshin, S.V., Dronov, D.O., Vorontsov, E.A., Balabanyan, V. Y., Posypanova, G.A., 2019. In vitro anticancer activity of folate-modified docetaxel-loaded PLGA nanoparticles against drug-sensitive and multidrug-resistant cancer cells. Cancer Nanotechnol. 10 https://doi.org/10.1186/s12645-019-0048-x.

Puzzo, M., De Santo, M., Morelli, C., Leggio, A., Pasqua, L., 2024. The Advent of Molecular Targeted Therapies Against Cancer. Toward Multi-Targeting Drugs Through Materials Engineering: A Possible Future Scenario. Small Science. DOI: 10.1002/smsc.202400113.

Qu, N., Lee, R.J., Sun, Y., Cai, G., Wang, J., Wang, M., Lu, J., Meng, Q., Teng, L., Wang, D., Teng, L., 2016. Cabazitaxel-loaded human serum albumin nanoparticles as a therapeutic agent against prostate cancer. Int. J. Nanomed. 11, 3451–3459. https://doi.org/10.2147/IJN.S105420.

Rafiei, P., Michel, D., Haddadi, A., 2015. Application of a Rapid ESI-MS/MS Method for Quantitative Analysis of Docetaxel in Polymeric Matrices of PLGA and PLGA-PEG Nanoparticles through Direct Injection to Mass Spectrometer. Am J Analyt Chem 06, 164–175. https://doi.org/10.4236/ajac.2015.62015.

Rivero-Buceta, E., Vidaurre-Agut, C., Vera-Donoso, C.D., Benlloch, J.M., Moreno-Manzano, V., Botella, P., 2019. PSMA-Targeted Mesoporous Silica Nanoparticles for Selective Intracellular Delivery of Docetaxel in Prostate Cancer Cells. ACS Omega 4, 1281–1291. https://doi.org/10.1021/acsomega.8b02909.

Rivero-Buceta, E., Encheva, M.E., Cech, B., Fernandez, E., Sastre, G., Landry, C.C., Botella, P., 2023. Light-activated controlled release of camptothecin by engineering porous materials: the ship in a bottle concept in drug delivery. Nanoscale 15, 12506–12517. https://doi.org/10.1039/d3nr00642e.

Scharmann, W., 1999. Physiological and ethological aspects of the assessment of pain, distress and suffering. Humane Endpoints in Animal Experiments for Biomedical Research 33–39.

Shaha, S., Rodrigues, D., Mitragotri, S., 2024. Locoregional drug delivery for cancer therapy: Preclinical progress and clinical translation. J. Control. Release. https://doi.org/10.1016/j.jconrel.2024.01.072.

Smith, B.D., Smith, G.L., Hurria, A., Hortobagyi, G.N., Buchholz, T.A., 2009. Future of cancer incidence in the United States: Burdens upon an aging, changing nation. J. Clin. Oncol. 27, 2758–2765. https://doi.org/10.1200/JCO.2008.20.8983.

Tang, X., Wang, G., Shi, R., Jiang, K., Meng, L., Ren, H., Wu, J., Hu, Y., 2016. Enhanced tolerance and antitumor efficacy by docetaxel-loaded albumin nanoparticles. Drug Deliv. 23, 2686–2696. https://doi.org/10.3109/10717544.2015.1049720.

Tanga, S., Aucamp, M., Ramburrun, P., 2023. Injectable Thermoresponsive Hydrogels for Cancer Therapy: Challenges and Prospects. Gels. https://doi.org/10.3390/gels9050418.

Tilki, D., Pompe, R.S., Bandini, M., Marchioni, M., Kretschmer, A., Tian, Z., Karakiewicz, P.I., Evans, C.P., 2018. Local treatment for metastatic prostate cancer: A systematic review. Int. J. Urol. 25, 390–403. https://doi.org/10.1111/iju.13535.

Walter, K.A., Tamargo, R.J., Olivi, A., Burger, P.C., Brem, H., 1995. Intratumoral chemotherapy. Neurosurgery 37, 1129–1145. https://doi.org/10.1227/00006123-199512000-00013.

Wang, W., Fan, J., Zhu, G., Wang, J., Qian, Y., Li, H., Ju, J., Shan, L., 2020. Targeted prodrug-based self-assembled nanoparticles for cancer therapy. Int. J. Nanomed. 15, 2921–2933. https://doi.org/10.2147/IJN.S247443.

Xu, Q., Yang, Y., Lu, J., Lin, Y., Feng, S., Luo, X., Di, D., Wang, S., Zhao, Q., 2022. Recent trends of mesoporous silica-based nanoplatforms for nanodynamic therapies. Coord. Chem. Rev. https://doi.org/10.1016/j.ccr.2022.214687.

Yoo, G.H., Subramanian, G., Boinpally, R.R., Iskander, A., Shehadeh, N., Oliver, J., Ezzat, W., Piechocki, M.P., Ensley, J.F., Lin, H.S., Shibuya, T.Y., Polin, L., Parchment, R.E., 2005. An in vivo evaluation of docetaxel delivered intratumorally in head and neck squamous cell carcinoma. Arch. Otolaryngol. Head Neck Surg. 131, 418–429. https://doi.org/10.1001/archotol.131.5.418.

Yoo, G.H., Subramanian, G., Ezzat, W.H., Tulunay, O.E., Tran, V.R., Lonardo, F., Ensley, J.F., Kim, H., Won, J., Stevens, T., Zumstein, L.A., Lin, H.S., 2010. Intratumoral delivery of docetaxel enhances antitumor activity of Ad-p53 in murine head and neck cancer xenograft model. Am. J. Otolaryngol. Head Neck Med. Surg. 31, 78–83. https://doi.org/10.1016/j.amjoto.2008.10.002.

Yu, M., Zhang, C., Tang, Z., Tang, X., Xu, H., 2019. Intratumoral injection of gels containing losartan microspheres and (PLG-g-mPEG)-cisplatin nanoparticles improves drug penetration, retention and anti-tumor activity. Cancer Lett. 442, 396–408. https://doi.org/10.1016/j.canlet.2018.11.011.

Yun, W.S., Kim, J., Lim, D.K., Kim, D.H., Jeon, S.I., Kim, K., 2023. Recent studies and progress in the intratumoral administration of nano-sized drug delivery systems. Nanomaterials. https://doi.org/10.3390/nano13152225.

Zhang, W., Fan, W., Rachagani, S., Zhou, Z., Lele, S.M., Batra, S.K., Garrison, J.C., 2019. Comparative study of subcutaneous and orthotopic mouse models of prostate cancer: vascular perfusion, vasculature density, hypoxic burden and BB2r-targeting efficacy. Sci. Rep. 9, 11117. https://doi.org/10.1038/s41598-019-47308-z.

Zhao, M., Su, M., Lin, X., Luo, Y., He, H., Cai, C., Tang, X., 2010. Evaluation of docetaxel-loaded intravenous lipid emulsion: Pharmacokinetics, tissue distribution, antitumor activity, safety and toxicity. Pharm. Res. 27, 1687–1702. https://doi.org/10.1007/s11095-010-0180-0.

Zhao, X., Zhao, Y., Geng, L., Li, X., Wang, X., Liu, Z., Wang, D., Bi, K., Chen, X., 2011. Pharmacokinetics and tissue distribution of docetaxel by liquid chromatography-mass spectrometry: Evaluation of folate receptor-targeting amphiphilic copolymer modified nanostructured lipid carrier. J. Chromatogr. B Analyt. Technol. Biomed. Life Sci. 879, 3721–3727. https://doi.org/10.1016/j.jchromb.2011.10.015.